



Hydrothermal Synthesis of Gadolinium (Gd) Doped Cerium Oxide (CeO₂) Nanoparticles: Characterization and Antibacterial Activity

Y. A. SYED KHADAR^{1*}, A. BALAMURUGAN², V.P. DEVARAJAN¹ and R. SUBRAMANIAN³

¹Department of Physics, K.S.R. College of Arts and Science for Women, Tiruchengode, Namakkal - 637 215, Tamil Nadu, India.

²Department of Physics, Government Arts College, Udhagamandalam, Namakkal - 637 215, Tamil Nadu, India.

³Department of Chemistry, K.S.Rangasamy College of Arts and Science, Tiruchengode, Namakkal - 637 215, Tamil Nadu, India.

*Corresponding author E-mail: syedkhadar_ya@yahoo.co.in

<http://dx.doi.org/10.13005/ojc/330533>

(Received: July 08, 2017; Accepted: August 20, 2017)

ABSTRACT

This present study has been described the synthesis, characterization and antibacterial activity of gadolinium doped cerium oxide nanoparticles. The nanoparticles were prepared by hydrothermal method with various concentrations of gadolinium ranges from 2 mol% to 8 mol%. The X-ray diffraction (XRD) pattern revealed the face-centered cubic structure with crystalline size of 58.3 nm to 57.4 nm with increasing the concentration of gadolinium (2 mol% to 8 mol%). The Ce-O chemical bonding nature was confirmed using Fourier transform infrared spectrometer (FTIR). The field emission scanning electron microscope (FESEM) exhibited fascinating shapes like cube and square of nanoparticles. UV spectrophotometer used to measure the optical behaviors of CeO₂ nanoparticles. Band-edge absorption of CeO₂ nanoparticles blue shifted upon increasing the gadolinium concentration as compared to undoped CeO₂ nanoparticles. The emission behavior of nanoparticles was examined by photoluminescence (PL) spectroscopy. PL spectra reveals a peak shift of CeO₂ emission upon gadolinium doped due to oxygen defect. The gadolinium doped CeO₂ nanoparticles showed better antibacterial activity against the pathogenic bacteria such as *Escherichia coli*, *Staphylococcus aureus*, *Bacillus cereus* and *Salmonella typhi*.

Keyword: CeO₂ Nanoparticles; Hydrothermal method; Morphology; Antibacterial activity.

INTRODUCTION

Cerium oxide (CeO₂) nanostructures are getting more familiarity due to its enhanced properties than that of bulk material¹. The cerium

oxide nanoparticles (CeO₂NP_s) have unique structure because of their broad applicability to various areas such as microelectronics, optoelectronics, fuel cell technologies, gas sensors, solid state electrolytes and antimicrobial activities²⁻⁴. There are

several methods have been proposed for the synthesis of CeO₂ nanoparticles⁵⁻⁸. The hydrothermal method has advantages over other methods such as efficient synthesis process and morphology controlled growth. The CeO₂ NP_s played an important role in the remediation of toxicity of microorganism such as bacteria, yeast and fungi⁹. At lower temperatures it was found that this material has antimicrobial activity against several bacteria and reported the microorganisms were destroyed by the possibility of generation of reactive oxygen species¹⁰. The CeO₂ nanoparticles and cell membrane of bacteria are attracted with each other due to the electrostatic interaction nature. Hence, this interaction indicates the important role of medium charge and microorganism surface nature in the antibacterial activity¹¹. Further, the doping effect enhances the physical properties of CeO₂ nanostructures for environment remediation. However, there is lack of information on the effect of Gadolinium (Gd) dopants on the structure and morphology in comparison with the undoped ceria. Considering the physical and chemical properties of CeO₂ NPs, we made an attempt to synthesis the Gd doped CeO₂ NPs by hydrothermal method. The undoped and Gd doped CeO₂ nanoparticles were characterized using various structural and spectral techniques. Antibacterial properties of these samples were determined against four pathogenic bacteria to know its bacterial killing efficiencies.

EXPERIMENTAL

Synthesis of Gd doped CeO₂ nanoparticles

Trisodium phosphate solution (0.02 M), 20 ml was slowly drop wise added to 60 ml of 0.1 M solution of cerium nitrate under magnetic stirring. During meanwhile 2, 4, 6, and 8% of gadolinium nitrate solution were added to the above reaction mixture and continuously stirred for 30 min. The reaction mixture under constant stirring was resulted as white colloid. Then, the colloids were transferred to the Teflon coated autoclave vessel (100 ml capacity) for hydrothermal treatment maintained at 180 °C for 15 hr. The autoclave vessel was cooled to room temperature. The colloid was removed by centrifugation and thoroughly washed with double

distilled water followed by ethanol and dried at 60 °C for 5 hr. A blank sample (CeO₂) synthesized without gadolinium using the same procedure at same experiment conditions for the purpose of comparison.

Investigation of Nanoparticles

The crystal structure of CeO₂ and Gd doped CeO₂ nanoparticles were determined by powder X-ray diffraction technique. XRD patterns were recorded using X-ray diffractometer (XRD, Shimadzu-6000) using CuK α radiation ($\lambda=1.5408$ Å). The surface morphology of CeO₂ and Gd doped CeO₂ nanoparticles were studied using a scanning electron microscope (SEM, JOEL JSM-6390). The presence of functional groups was confirmed using Fourier transform infrared spectrometer (FTIR, Bruker-Tensor 27). UV-absorption spectra of synthesized nanoparticles were carried using spectrophotometer UV-Vis (UV-Vis, Jasco V530). The photoluminescence (PL) emission spectra were measured at an excitation wavelength of 340 nm using Photoluminescence spectroscopy (Horiba Jobin, Fluoromax-4) at room temperature.

Antibacterial Activity of Gd doped CeO₂

The antibacterial activity of CeO₂ and Gd doped CeO₂ nanoparticles were studied against pathogenic bacteria such as *Escherichia coli*, *Staphylococcus aureus*, *Bacillus cereus* and *Salmonella typhi* using agar disc diffusion method. For this study, CeO₂ and Gd doped CeO₂ nanoparticles were prepared at the concentration of 1 mg/ml using dimethylsulfoxide (DMSO) as solvent¹². Then, the dispersed nanoparticles were impregnated into each sterile disc using micropipette under aseptic condition. The overnight bacterial culture was prepared using sterile nutrient broth. Then, all the grown bacterial culture was aseptically transferred to the sterile Mueller-Hinton agar medium using sterile cotton swab. After, the impregnated discs were kept on culture swapped Mueller Hinton Agar medium using sterile forceps. Finally, all the inoculated plates were allowed to incubate for 24 h. using bacteriological incubator. After incubation, the zone of inhibition was measured against the bacterial strains.

RESULTS AND DISCUSSION

FTIR Functional group studies

A broad peak observed at 3357 cm^{-1} is attributed to the OH stretching vibrations of moisture content present in atmosphere¹³. The band obtained at 2424 and 1042 cm^{-1} are due to the presence of organic impurities in the sample. The peak at 2424 cm^{-1} is due to the presence of dissolved or atmospheric CO_2 in the samples. A sharp peak obtained at 1629 cm^{-1} corresponds to the bending vibrations of H-O-H which is partly overlapping the O-C-O bond¹⁴. A band at 1379 cm^{-1} is due to the N-O stretching vibrations of oxygen atom present in the ceria nanoparticles. A peak noticed at 818 cm^{-1} is attributed to the O-Ce-O bonding nature of ceria nanoparticles. The small bands obtained at 700 , 615 and 545 cm^{-1} are corresponding to Ce-O stretching mode¹⁵. Thus FTIR spectra of the samples confirm the formation of Gd-CeO₂ nanoparticles.

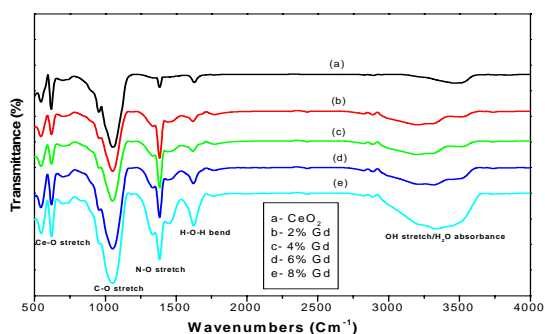


Fig. 1. FTIR spectrum of (a) undoped CeO₂, (b) 2mol % Gd, (c) 4mol % Gd, (d) 6mol % Gd and (e) 8mol % Gd doped CeO₂ nanoparticles.

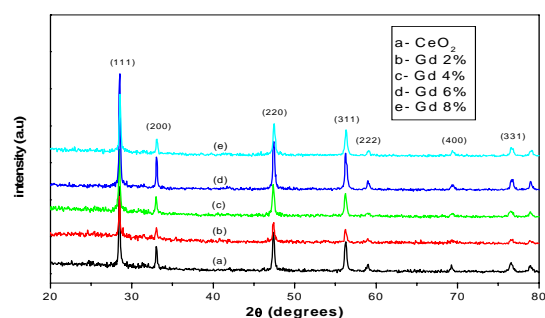


Fig. 2. XRD pattern of (a) undoped CeO₂, (b) 2mol % Gd, (c) 4mol % Gd, (d) 6mol % Gd and (e) 8mol % Gd doped CeO₂ nanoparticles.

XRD structural studies

The crystal structure, grain size and the lattice parameters of Gd-CeO₂ NPs were analyzed from the XRD spectra is shown in Fig. 2. The XRD

pattern of the Gd-CeO₂ NPs is well indexed with the standard data [JCPDS card no. 75-0162]¹⁶. The XRD pattern reveals the crystalline nature of the synthesized Gd-CeO₂ nanoparticles. The peaks obtained at 2θ values at 28.5 , 33.0 , 47.4 , 56.3 , 59.0 , 69.4 , and 76.7° are corresponding to the (1 1 1), (2 0 0), (2 2 0), (3 1 1), (2 2 2), (4 0 0) and (3 3 1) planes. Our result is similar with the existing literature data of the CeO₂¹⁷.

In Gd doped CeO₂ NPs, the 2θ value of (111) plane is shifted towards lower side when the concentrations of Gd is increased. It happened due to the replacement of dopant ion in the CeO₂ lattice¹⁸. In addition, the peak broadening taken place in Gd doped CeO₂ nanoparticles as compared with that of pure CeO₂ synthesized without Gd. The broadening of the peak in Gd doped CeO₂ NPs clearly indicates the smaller sized particles as shown in Fig.2. The average crystallite size calculated using Debye-Scherrer's formula was found in the range between 57.4 - 58.3 nm ¹⁹. The size of Gd doped CeO₂ nanoparticles decreased with increasing the concentration of Gd²⁰. The average sizes of Gd-CeO₂ NPs are summarized in Table1.

Table. 1: XRD content for undoped and Gd doped CeO₂ nanoparticles.

Samples	2θ (deg)	Crystallite size (nm)	d-spacing (Å)
CeO ₂	28.53	58.24	3.126
CeO ₂ : Gd (2%)	28.47	57.99	3.134
CeO ₂ : Gd (4%)	28.48	57.85	3.131
CeO ₂ : Gd (6%)	28.45	57.56	3.132
CeO ₂ : Gd (8%)	28.51	57.40	3.132

Optical studies

UV-Vis absorption spectra of as-synthesized and Gd doped CeO₂ nanoparticles are shown in Fig 3. The as-synthesized CeO₂ nanoparticles show a strong absorption peak at 345 nm . Its corresponding bandgap energy (E_g) obtained is 3.62 eV was calculated using $E_g = 1242/\lambda_{\text{absorption}}$ relationship. The bandgap energy found to be slightly increased to 3.67 eV on increasing the concentration of Gd from $2\text{ mol } \%$ to $8\text{ mol } \%$. It is believed that the decreased in the size

of particles due to the increase of Gd concentration²¹. The absorption value reveals the charge transfer from O^{2-} to Ce^{4+} energy levels in CeO_2 crystal lattice²². The absorption wavelength and their corresponding bandgap energy values are presented in Table 2.

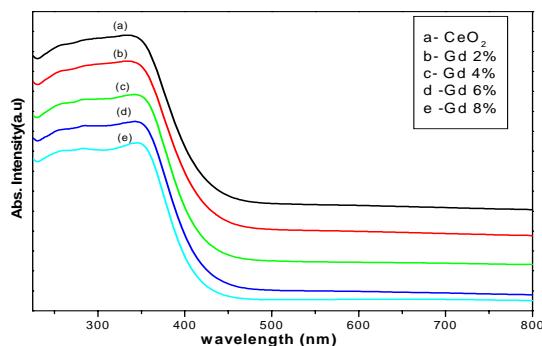


Fig. 3. UV absorption spectra of (a) undoped CeO_2 , (b) 2mol % Gd, (c) 4mol % Gd, (d) 6mol % Gd and (e) 8mol % Gd doped CeO_2 nanoparticles

Table 2: Bandgap energy for undoped and Gd doped CeO_2 nanoparticles.

Samples	Abs. Wavelength (nm)	Band gap energy (eV)
CeO_2	343	3.62
CeO_2 : Gd (2mol %)	341	3.64
CeO_2 : Gd (4mol %)	340	3.65
CeO_2 : Gd (6mol %)	339	3.66
CeO_2 : Gd (8mol %)	338	3.67

PL emission Studies

spectra of Gd doped CeO_2 nanoparticles are revealed in Fig. 4. All Gd doped CeO_2 samples showed excitation at 340 nm²³. As-synthesized sample showed strong emission peak at 377 nm and it resembles to the transition of electron from localized Ce_{2f} state to valence band of O_{2p} . In addition, an emission peak at 434 nm and 466 nm was originated from defect states widely existing between Ce_{4f} states to O_{2p} of valence band. Moreover, an emission nature was gradually decreased beyond the range of 470 nm and also it was extended upto 550 nm. This emission range is related to charge transfer from Ce_{4f} energy level to O_{2p} level of valence band. Similarly, from the Gd doped CeO_2 nanoparticles, the localized Ce_{4f} state to O_{2p} of valence band transition related emission nature is taken place gradually decreased due to

Gd ions in the CeO_2 crystal lattice causes doping effect.

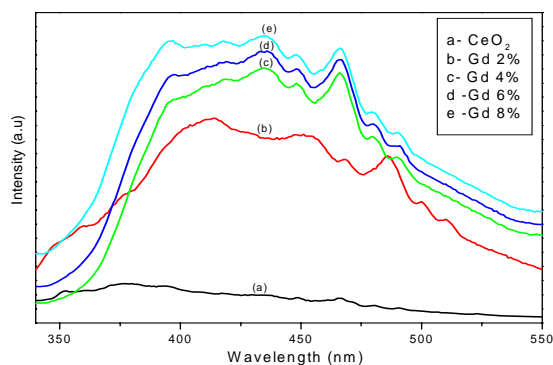


Fig. 4. PL emission spectra of (a) undoped CeO_2 , (b) 2mol % (c) 4mol % (d) 6mol % and (e) 8mol % Gd doped CeO_2 nanoparticles.

On the other hand, the emission band of Gd doped CeO_2 NPs gradually shifted towards longer wavelength, like 414, 454 and 486 nm as compared with that of as-synthesized CeO_2 nanoparticles. This emission range is related to charge transfer from Ce_{4f} energy level to O_{2p} level of valence band and also possibility occurred due to the attribution of oxygen defects. In steps of increased doping concentration 2 mol%, 4 mol%, 6 mol%, and 8 mol%, respectively, the emission peaks became red-shifted due to the formation of more oxygen defects or possibility of conducive conditions for Ce^{3+} formation. Previous reports suggest that increasing the Gd dopant concentration may increase surface defect levels and suppress the electron transfer from Ce_{4f} to O_{2p} levels²⁴.

SEM morphology studies

The images of pure CeO_2 exhibit well defined cube and square shape uniform sized particles. The particles are uniformly dispersed. However, some distortion found in the Gd doped CeO_2 nanoparticles. Four samples (CeO_2) were synthesized using 2, 4, 6 and 8 mol% of Gd.

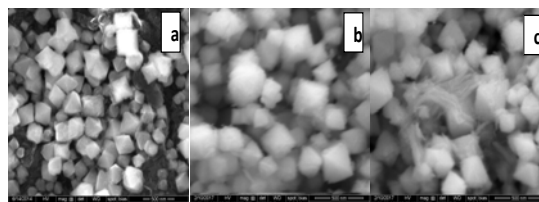


Fig. 5. SEM images of (a) undoped CeO_2 , (b) 2mol % Gd (c) 8mol % Gd doped CeO_2 nanoparticles.

Among four samples, two samples synthesized using 2 mol% (low concentration) 8 mol% (high concentration) of Gd were characterized as representative samples. As shown in Fig 5 (a) pure CeO₂NPs show well defined shaped cubic crystals. The particles in the images are uniformly distributed. The cubic crystalline structure of 2 mol% Gd doped CeO₂ show slight distortion in its structure Fig.5 (b). Similarly, the crystalline structures of CeO₂ nanocrystals are evenly distributed during the doping of 8 mol% Gd with slight distortion Fig. 5 (c). It is clearly reveals that the addition of Gd to CeO₂ slightly changed the morphology of CeO₂. The appearance of feather like fibre on the surface of cubic CeO₂ nanocrystals indicate the effect of Gd in the formation of CeO₂ crystal lattice²⁵.

Evaluation of Antibacterial activity

Antibacterial activity of undoped and Gd doped CeO₂ nanoparticles were evaluated against pathogenic bacteria such as *Escherichia coli*, *Staphylococcus aureus*, *Bacillus cereus* and *Salmonella typhi*. The antibacterial results of nanoparticles are shown in Fig. 6. The average zone of inhibition exhibited by pure CeO₂ and various concentration of Gd doped CeO₂ nanoparticles are presented in Table 3. The pure CeO₂NP_s did not show any activity against four

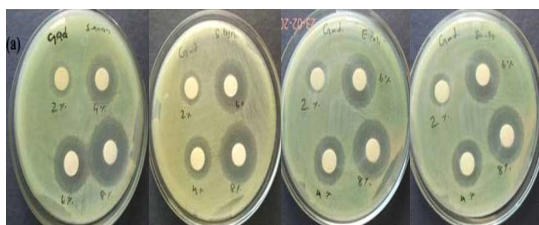


Fig. 6. Anti-bacterial activity of Gd doped CeO₂ nanoparticles with different bacterial strains.

bacteria. Whereas, the Gd doped CeO₂ nanoparticles showed good antibacterial activity. The result obtained from the antibacterial study reveals that the killing efficiency of Gd doped CeO₂NP_s increased with increasing the concentration of Gd²⁶. The zone of inhibition clearly show that the killing potential of CeO₂ significantly increased by the Gd doping with Gd doped CeO₂.

The 2 mol% Gd doped CeO₂ showed 13, 13, 15 and 15 mm zone of inhibition against *E.coli*, *B.cereus*, *S. aureus* and *S. typhi*, respectively. After increasing the concentration of Gd to 4 mol%, the antibacterial activity against the same bacteria increased to 19, 19, 18 and 28 mm. In 6 mol%, the measured zone of inhibition was 24, 23, 21 and 24 mm. As shown in Table 3, 8 mol% of Gd doped CeO₂NP_s showed maximum zone of inhibition against all those bacteria as 28, 26, 23 and 26 mm. Among the four tested samples, 8 mol% Gd doped CeO₂ nanoparticles exhibit maximum bacterial activity against *E.coli*. Finding new biomaterials to kill such bacteria is a needy one. The increased concentration of Gd doping with CeO₂ increases the antibacterial activity. It is due to the decreased particle size and increased surface to volume ratio.

It is noted that the bandgap energy of the samples increased with increasing the concentration of Gd. Similarly, emission spectra of the Gd doped CeO₂NP_s shifted towards longer wavelength as compared with pure CeO₂NP_s. In XRD pattern, the particle size decreases with increasing the concentration of Gd. The antibacterial activity of the Gd doped CeO₂NP_s found to be increased with increasing the concentration of Gd. The formation of Gd doped CeO₂NP_s reveals the crystalline and smaller sized nanoparticles. As the band gap energy increases, the particle size

Table. 3: Antibacterial activity for Gd doped CeO₂ nanoparticles

Bacterial strains	Zone of Inhibitions (mm)			
	Various Concentrations of Gadolinium			
	2mol %	4mol %	6mol %	8mol %
<i>E. coli</i>	13 mm	19 mm	24 mm	28 mm
<i>B. cereus</i>	13 mm	19 mm	23 mm	26 mm
<i>S. aureus</i>	15 mm	18 mm	21 mm	23 mm
<i>S. typhi</i>	15 mm	21 mm	24 mm	26 mm

decreases, thus Gd doping produce smaller CeO₂NP_s nanoparticle. The smaller size particles easily transmit into the cell walls. It also increases the interaction between nanoparticle and the outer surface of the bacteria which induce more toxicity to the bacteria. Hence the Gd doped CeO₂NP_s showed maximum zone of inhibition against pathogenic bacteria.

CONCLUSIONS

Pure CeO₂ and Gd doped CeO₂NP_s were successfully synthesized. A face-centre cubic crystal structure was confirmed from XRD patterns and their calculated crystalline sizes were 57.4 - 58.3 nm. A

blue-shifted absorption was observed from UV optical spectrum and their calculated bandgap energy values were 3.62 - 3.67 eV. The Ce-O chemical bonding nature and the presence of functional groups were confirmed from FTIR spectrum. A cube shaped surface morphology was observed from FESEM images. Further, the antibacterial activity of nanoparticles were studied against different types of bacteria and observed enhanced killing effects. From the overall observations, we have concluded that the increasing concentration of Gd doping from 2 mol% to 8 mol% has shown an enhanced results such as decreased crystalline size, morphology change and antibacterial activity.

REFERENCES

- Sun, C.; Li H.; Chen, L. *Energy Environ. Sci.* **2012**, *5*, 8475
- Semikina, T.V. *Semicond Phys Quantum Electron Optoelectron.* **2004**, *7*, 291-296.
- Jasinski, P.; Suzuki, T.; Anderson, H.U. *Sens. Actuator B Chem.* **2003**, *95*, 73-77.
- Lu, X.; Zhai, T.; Cui, H.; Shi, H.; Xie, S.; Huang, Y.; Liang, C.; Tong, Y. *J. Mater. Chem.* **2011**, *21*, 5569-5572.
- Liu, Y. H.; Zuo, J. C.; Ren, X. F.; Yong, L. *Metallurgy.* **2014**, *53*, 463-465.
- Bumajdad, A.; Eastoe, J.; Mathew, A. *Adv. Colloid Interface Sci.* **2009**, *147*, 56-66.
- Yuan, Q.; Duan, H. H.; Li, L. L.; Sun, L. D.; Zhang, Y. W.; Yan, C. H. *J. Colloid Interface Sci.* **2009**, *335*, 151-167.
- Zamiri, R.; Ahangar, H. A.; Kaushal, A.; Zakaria, A.; Zamiri, G.; Tobaldi, D.; Ferreira, J. M. F. *PLoS One.* **2015**, *10*, e0122989.
- Masui, T.; Fujiwara, K.; Machida, K. I.; Adachi, G. Y.; Sakata, T.; Mori, H. *Chem. Mater.* **1997**, *9*, 2197-2204.
- Santos, C. L.; Albuquerque, A. J. R.; Sampaio, F. C.; Keyson, D. Volume 4, Microbiology Book Series: Formatex Research Center, Badajoz, Spain **2013**.
- Thill, A.; Zeyons, O.; Spalla, O.; Chauvat, F.; Rose, J.; Auffan, M.; Flank, A. M. *Environ. Sci. Technol.* **2006**, *40*, 6151-6156.
- Azad, A. M.; Matthews, T.; Swary, J. *Mater. Sci. Eng. B.* **2005**, *123*, 252-258.
- Qizheng, C.; Xiangting, D.; Jinxian, W.; Mei, L. *J. Rare earth.* **2008**, *26*, 664-669.
- Li, D.; Xia, Y. *Nano Lett.* **2004**, *4*, 933-938.
- Wang, T.; Sun, D. C. *Mater. Res. Bull.* **2008**, *43*, 1754-1760.
- Jadhav, L. D.; Chourashiya, M. G.; Jamale, A. P.; Chavan, A. U.; Patil, S. P. *J. Alloys Comp.* **2010**, *506*, 739-744.
- Zarinkamar, M.; Farahmandjou, M.; Firoozabadi, T. P. *J. Ceram. Process. Res.* **2016**, *17*, 166-169.
- Srinivas, K.; Vithal, M.; Sreedhar, B.; Raja, M.; Reddy, P. *J. Phys. Chem. C.* **2009**, *113*, 3543-3552.
- Bear, J. C.; McNaughten, P. D.; Southern, P.; Brien, P.; Dunnill, C. W. *Crystal.* **2015**, *5*, 312-326.
- Taniguchi, T.; Watanabe, T.; Sugiyama, N. J. *Phys. Chem C.* **2009**, *113*, 19789-19793.
- Hu, C.; Zhang, Z.; Liu, H.; Gao, P.; Wang, Z. L. *Nanotechnol.* **2006**, *17*, 5983-5987.
- Saranya, J.; Ranjith, K. S.; Saravanan, P.; Mangalaraj, D.; Rajendra Kumar, R. T. *Mater. Sci. Semicond Proc.* **2014**, *26*, 218-224.
- Babitha, K. K.; Sreedevi, A.; Prinkaya, K. P.; Sabu, B.; Vargheze, T. *J. Pure Appl. Phys.* **2015**, *53*, 596-603.
- Ranjith, K. S.; Saravanan, P.; Chen, S. H.; Dong, C. L.; Chen, C. L.; Chen, S. Y.; Asokan, K.; Rajendra Kumar, R. T. *J. Phys. Chem. C.* **2014**, *118*, 27039-27047.
- Liu, Y.; Li, T.; Chen, W.; Guo, Y.; Liu, L.; Guo, H. *RSC Adv.* **2015**, *5*, 11733-11737.

26. Gopinath, K.; Karthika, V.; Sundaravadivelan, C.; Gowri, S.; Arumugam, A. *J. Nanostruct. Chem.*, **2015**, *5*, 295-303.
27. Ravi kumar, S.; Gokulakrishnan, R.; Boomi, R. *Asian Pac. J. Trop. Dis.* **2012**, *2*, 85-89.
28. Leung, Y.H.; Yung, M. M. N.; Ng, A. M. C.; Ma, A. P. Y.; Wong, S. W. Y.; Chan, C. M. N.; Ng, Y. H.; Djuricic, A. B.; Guo, M.; Wong, M. T.; Leung, F. C. C.; Chan, W. K.; Leung, K. M. Y.; Lee, H. K. *J. Photochem. Photobiol. B.* **2015**, *145*, 48-59.
29. Kuang, Y.; He, X.; Zhang, Z.; Li, Y.; Zhang, H.; Ma, Y.; Wu, Z.; Chai, Z. *J. Nanosci. Nanotechnol.* **2011**, *11*, 4103.1